ACS APPLIED MATERIALS & INTERFACES

Research Article

www.acsami.org

Hierarchically Structured Manganese Oxide-Coated Magnetic Nanocomposites for the Efficient Removal of Heavy Metal Ions from Aqueous Systems

Eun-Ju Kim,[†] Chung-Seop Lee,[†] Yoon-Young Chang,[‡] and Yoon-Seok Chang*[,†]

[†]School of Environmental Science and Engineering, Pohang University of Science and Technology (POSTECH), Pohang 790-784, Republic of Korea

[‡]Department of Environmental Engineering, Kwangwoon University, Seoul 139-701, Republic of Korea

Supporting Information

ABSTRACT: In this study, hierarchical MnO_2-coated magnetic nanocomposite (Fe_3O_4/MnO_2) was synthesized by a mild hydrothermal process, and its application for removing heavy metal ions from contaminated water systems was examined. Structural characterization showed that the Fe_3O_4 nanoparticle core was coated with amorphous MnO_2 shell with flowerlike morphology. The as-prepared nanocomposite had a large surface area and high magnetic saturation value, which ensured its good sorption ability and convenience of separation. Fe_3O_4/MnO_2 exhibited a greatly improved removal capacity toward four different heavy metals (Cd(II), Cu(II), Pb(II), and Zn(II)) compared to unmodified Fe_3O_4 nanoparticles. The adsorption property of Fe_3O_4/MnO_2 was studied with Cd(II) in more detail. The sorption equilibrium data were well fitted to the Langmuir model, and the maximum adsorption capacity toward Cd(II) was 53.2 mg g^{-1}. Fe_3O_4/MnO_2 retained over 80% of its adsorption capacity under various solution conditions that are typically encountered in natural waters. This nanocomposite was easily recovered and reused through consecutive adsorption−desorption experiments with the assistance of an external magnetic field. Overall, the findings propose that Fe_3O_4/MnO_2 could be used as an effective recyclable adsorbent for heavy metal ions.

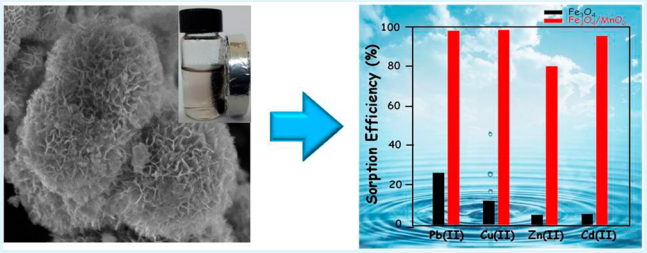

KEYWORDS: *manganese oxides, iron oxide nanoparticles, heavy metal ions, magnetic separation, recyclable adsorbent*

1. INTRODUCTION

Heavy metal ion removal from water effluents has attracted much attention because of their detrimental effects on ecological systems and human health.[1] There have been a number of approaches to remove heavy metals, including chemical precipitation,[2,3] ion exchange,[4] membrane filtration,[5] and adsorption.[6−8] Of these techniques, adsorption is considered to be one of the most suitable and effective choices.[9−13] In comparison to other adsorbents under investigation, nanostructured adsorbents exhibit remarkably enhanced sorption capacity owing to their high surface-to-volume ratio. During the last 2 decades, various nanosized adsorbents have been prepared and adopted for water decontamination, (i.e., CeO_2 nanoparticles,[14] fullerenes,[15] silica hollow nanospheres,[16] Al_2O_3 and MgO nanoparticles,[17] etc). However, such nanomaterials still suffer from issues involving separation inconvenience from the wastewater. Thus, the development of new nanoadsorbents with a facile separation property is of great interest.

For this purpose, iron oxide nanoparticles, in particular magnetite (Fe_3O_4) and maghemite (γ-Fe_2O_3), have been extensively applied in designing nanoadsorbents because they have a large surface area and high magnetic susceptibility.[18] These nanoparticles are attracted to an external magnetic field but lose magnetism as the applied field is removed, which allows their fast and convenient isolation in the processing and recovery stages. Over the past few years, much work has been done to functionalize magnetic nanoparticles by coating them with inorganic materials,[19] polymers,[20,21] carbon,[22,23] and biomolecules.[24,25] Proper surface functionalization can prevent the agglomeration of magnetic nanoparticles and enhance their stability and sorption capacity. In this respect, it is highly desirable to explore new functional materials that can compensate for the limitations of naked magnetic nanoparticles, with a low cost and environmentally benign nature.

Recent studies have noted that oxide minerals, ubiquitous in soils and sediments, serve as natural sinks for contaminants in the environment.[26,27] Nanosized manganese oxides (MnO_2) are among the most reactive minerals that have high surface area, strong oxidizing/adsorptive abilities, and good stability under acidic conditions.[28] It is reported that MnO_2 attenuates numerous heavy metal ions via adsorption, ion-exchange, or

Received: July 2, 2013
Accepted: September 12, 2013
Published: September 12, 2013

   dx.doi.org/10.1021/am402615m | ACS Appl. Mater. Interfaces 2013, 5, 9628−9634

coprecipitation. Therefore, the modification of the Fe_3O_4 surface with MnO_2 is anticipated to increase the removal efficiency of the magnetic nanoparticles for heavy metal ions. By simultaneously taking advantage of the Fe_3O_4 core and MnO_2 shell as well as its mesoporous structure, MnO_2-coated Fe_3O_4 nanoparticles can be an ideal material with great potential to be used in environmental remediation. Despite the promising merits of MnO_2, there are only a few reports on its use in the functionalization of magnetic particles.[29] Although previous research has highlighted the advantages of MnO_2 coating for metal-ion adsorption, they looked into the sorption percentage without a deep investigation into the mechanism and experimental parameters. In addition, no study has focused on the recyclability of MnO_2-coated magnetic particles in wastewater treatment.

In the present study, hierarchically structured MnO_2-coated Fe_3O_4 nanocomposites (Fe_3O_4/MnO_2) were synthesized and characterized in detail. The obtained magnetic composites were used to extract heavy metal ions (Cu(II), Pb(II), Zn(II), and Cd(II)) from aqueous systems. The overall performance of Fe_3O_4/MnO_2 was assessed in terms of sorption kinetics, isotherms, and the effects of various geochemical parameters (solution pH, ionic strength, coexisting ions, and presence of natural organic matter). Considering their practical application, the regeneration and reusability of Fe_3O_4/MnO_2 was also examined.

2. EXPERIMENTAL SECTION

2.1. Materials and Reagents. The chemicals used in the experiments were of analytical grade and were obtained from Sigma-Aldrich. All stock solutions were prepared by dissolving chemicals (NaCl, $CaCl_2{\cdot}2H_2O$, $MgCl_2{\cdot}6H_2O$, $NaNO_3$, Na_2SO_4, Na_2HPO_4, $ZnCl_2$, $PbCl_2$, $CuCl_2{\cdot}2H_2O$, and $CdCl_2{\cdot}2.5H_2O$) into deionized (DI) water. The humic acid (HA) stock solutions were prepared by dissolving Suwannee River humic acid powder (Standard II, International Humic Substances Society) in DI water, followed by filtration through a 0.45 μm cellulose acetate membrane (ADVANTEC) under vacuum. The concentration of HA was expressed as dissolved organic carbon (mg L^{-1} as DOC) using a total organic-carbon analyzer (TOC, Shimadzu TOC-V_{CSH}). Fe_3O_4 nanopowder (<50 nm particle size, ≥98% purity) was supplied from Sigma-Aldrich.

2.2. Preparation of Fe_3O_4/MnO_2 Nanocomposites. The magnetic composites were prepared via a simple hydrothermal process on the basis of a previous literature report[30] with some modifications. Typically, 0.51 g of $KMnO_4$ was first dissolved in 35 mL of DI water, and 0.7 mL of HCl (37 wt %) was then slowly added dropwise. After stirring for 15 min, 0.3 g of Fe_3O_4 was added into the solution. The mixture was transferred to a Teflon-lined autoclave (50 mL) and sealed to heat at 110 °C for 6 h. The obtained products were washed with DI water and ethanol and dried under vacuum at 60 °C for 12 h.

2.3. Characterization. The size and morphology of the products were examined by field-emission scanning electron microscopy (FESEM, JEOL-J840) and transmission electron microscopy (TEM, JEM-2200FS). The elemental compositions were determined by energy-filtered TEM (EFTEM) and inductively coupled plasma-atomic emission spectrometry (ICP-AES, IRIS-AP). X-ray diffraction (XRD) patterns were recorded on a PANalytical X'Pert diffractometer for crystalline phase identification. Magnetic measurement was performed on an XL-7 magnetic property measurement system. The Brunauer–Emmett–Teller (BET) surface area and pore size distribution were measured by N_2 adsorption and desorption using an ASAP 2010 system at 77 K. The zeta potentials and hydrodynamic size distributions were measured with a Zetasizer ELSZ-1000.

2.4. Batch Adsorption Experiment. Adsorption experiments were performed at pH 6.3 ± 0.1 and room temperature. Each batch experiment was conducted twice, and the data shown were the average values. Briefly, Fe_3O_4/MnO_2 (0.02 g) was added to 20 mL of a 10 mg/L Cu(II), Pb(II), Cd(II), and Zn(II) solution. For the equilibrium study, Cd(II) concentrations were varied in the range of 10–50 mg/L. After a specified time on a rolling mixer (15 rpm), the particles were separated magnetically, and the supernatant was analyzed by atomic absorption spectroscopy (AAS, SpectrAA-800).

To investigate the effects of pH, ionic strength, coexisting anions/cations, and HA concentration on the sorption of Cd(II), the solutions were varied with 0.1 M HCl or 0.1 M NaOH, NaCl, different electrolyte ions (Ca^{2+}, Mg^{2+}, NO_3^-, SO_4^{2-}, and HPO_4^{2-}), and HA, respectively. For the regeneration, the particles were immersed in 10 mL of a 0.01 M HCl solution for 1 h and washed with DI water to neutralize the composite. Regenerated Fe_3O_4/MnO_2 was used for adsorption in the succeeding cycles.

3. RESULTS AND DISCUSSION

3.1. Characterization of Fe_3O_4/MnO_2. Figure 1 displays typical SEM and TEM images of the as-obtained product. The

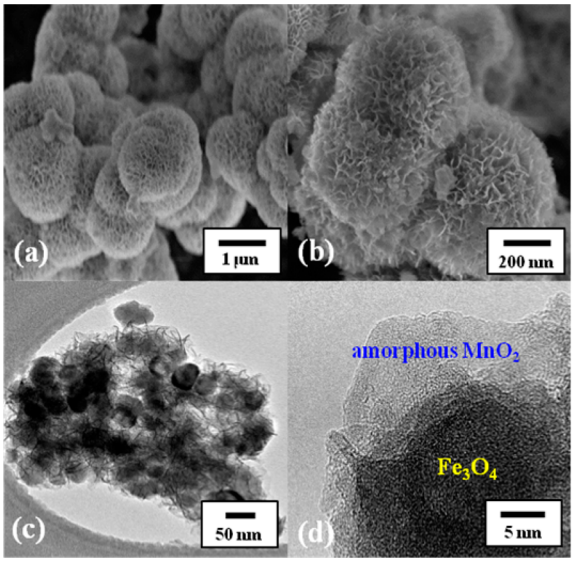

Figure 1. (a, b) SEM and (c, d) TEM images of Fe_3O_4/MnO_2.

low-magnification SEM image shown in Figure 1a gives an overview of the sample, revealing that the product is composed of many uniform flowerlike architectures. Further observation from high-magnification (Figure 1b) indicated that the flowery structure was the build up of many interleaving thin nanoplates. These nanoplates seemed to grow perpendicularly from a center. The TEM image of Figure 1c presents the aggregation of small flowerlike particles with a mean diameter of 60 nm. The average particle size, as measured in suspension by DLS, was about 218 nm (Figure S1, Supporting Information), which was larger than the size measured by TEM. The larger size determined by DLS compared to TEM was due to both aggregation and water solvation around the particles. A high-resolution TEM (HRTEM) is given in Figure 1d, in which an amorphous overlayer with a thickness of about 3–5 nm on the Fe_3O_4 core could be clearly identified. The elemental mapping images obtained from EFTEM exhibited MnO_2 shell structure, giving the distribution of the Mn element (Figure S2, Supporting Information). On the basis of the results of the HRTEM and EFTEM, it can be concluded that the as-prepared product consisted of Fe_3O_4 cores and amorphous MnO_2 shells (Fe_3O_4/MnO_2). According to ICP-AES analysis, the actual MnO_2 content was found to be ~35.8 wt % of the composite.

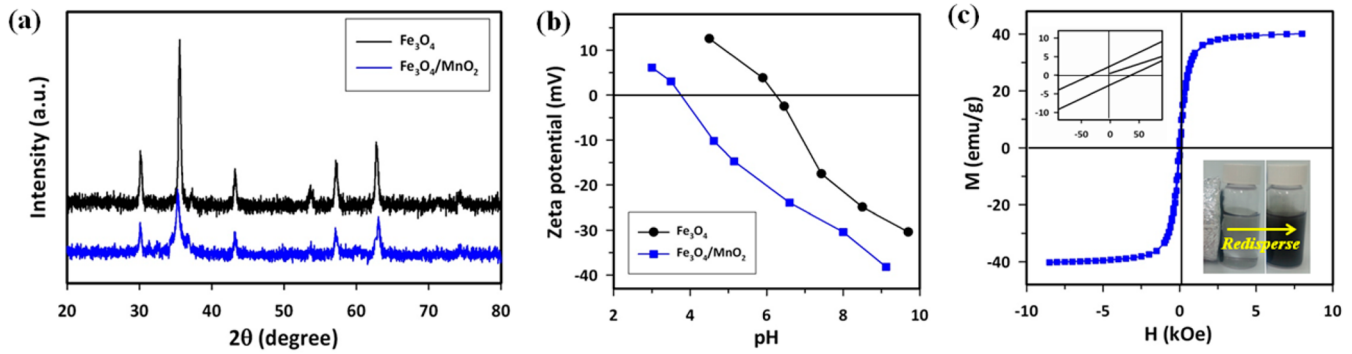

Figure 2. (a) XRD patterns of Fe_3O_4 and Fe_3O_4/MnO_2. (b) Zeta potentials of Fe_3O_4 and Fe_3O_4/MnO_2 as a function of pH in 1 mM $NaNO_3$. (c) Hysteresis loop of Fe_3O_4/MnO_2 at 300 K (top inset, expanded curve; bottom inset, photographs showing the magnetic separation and redispersion).

A series of additional measurements was also used to characterize Fe_3O_4/MnO_2. XRD patterns of bare Fe_3O_4 and Fe_3O_4/MnO_2 are shown in Figure 2a. The two patterns were similar, and all of the diffraction peaks were indexed as the face-centered cubic phases of Fe_3O_4. The results demonstrated that MnO_2 coating did not result in a phase change in the structure of the Fe_3O_4 nanoparticles. No peak assigned to the crystalline form of MnO_2 was detected, which could be explained by the amorphous nature of the outer MnO_2 layers. The respective zeta potentials of Fe_3O_4 and Fe_3O_4/MnO_2 were measured at varied pH (Figure 2b). The isoelectric point (IEP) for Fe_3O_4/MnO_2 was found to be around pH 3.7, which was much lower than that of Fe_3O_4 (pH 6.2). The low IEP value of Fe_3O_4/MnO_2 indicates that the composite facilitates more adsorption of positively charged heavy metal ions over a wide range of pH values. Figure 2c demonstrates the hysteresis loop of Fe_3O_4/MnO_2 at 300 K. The saturation magnetization (40 emu g^{-1}) of the composite was less than that reported for pure Fe_3O_4 nanocrystals, 70.7 emu g^{-1}.[31] However, this value was strong enough to achieve a facile magnetic separation. As shown in the inset photograph, Fe_3O_4/MnO_2 was rapidly collected within seconds from an aqueous suspension by an external magnetic field. In addition, the separated particles were easily redispersed with gentle shaking to a fairly stable suspension. This is essentially important for the convenient reuse of Fe_3O_4/MnO_2. The specific surface areas of pure Fe_3O_4 and Fe_3O_4/MnO_2 were calculated to be 56 and 118 m^2 g^{-1}, respectively. According to the pore size distribution (Figure S3, Supporting Information), Fe_3O_4/MnO_2 exhibited a mesoporous structure with an average diameter of 3.3 nm. The pores were likely due to the void surface of the self-assembled nanoparticles. The large surface area and mesoporous structure of Fe_3O_4/MnO_2 make them very promising candidates for the adsorption of pollutants in water purification.

3.2. Adsorption of Heavy Metal Ions. The MnO_2-coated magnetic nanocomposites were applied as adsorbents to remove heavy metal ions from water. Pure Fe_3O_4 was also studied for comparison. It was shown that the sorption reactions of the tested heavy metals (Cu(II), Pb(II), Zn(II), and Cd(II)) by Fe_3O_4/MnO_2 were very fast because the equilibrium was reached within 10 min. More than 95% of the Cu(II), Pb(II), and Cd(II) could be removed after 5 min. Such a fast adsorption could be attributed to the absence of internal diffusion resistance. The metal uptake capacities of Fe_3O_4 and Fe_3O_4/MnO_2 were shown in Figure 3, and Fe_3O_4/MnO_2 exhibited superior sorption efficiencies compared with those of Fe_3O_4. The relatively high adsorption capacity of Fe_3O_4/MnO_2 arises from their greater surface area (Fe_3O_4, 56 m^2 g^{-1}; Fe_3O_4/MnO_2, 118 m^2 g^{-1}), which contributes to the increase in the number of adsorption sites for metal ions.

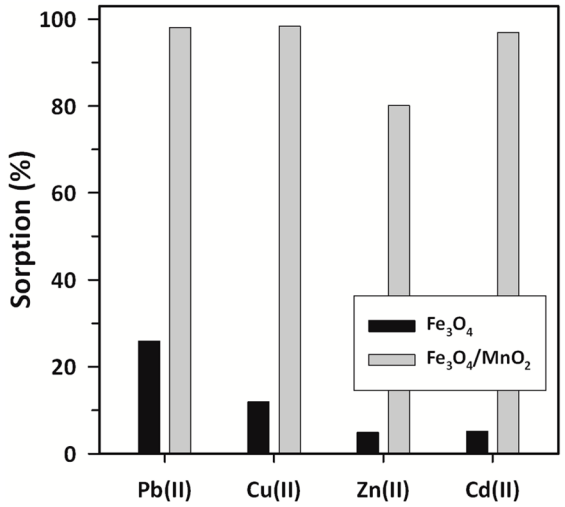

Figure 3. Sorption of Pb(II), Cu(II), Zn(II), and Cd(II) on Fe_3O_4/MnO_2. ([adsorbent], 1 g L^{-1}; [M(II)], 10 mg L^{-1}; pH 6.3 ± 0.1; contact time, 0.5 h).

The sorption kinetics fitted very well to a pseudo-second-order model (eq 1), and the obtained kinetic parameters are listed in Table 1.

$$\frac{t}{q_t} = \frac{1}{k_2 q_e^{\,2}} + \frac{t}{q_e} \quad (1)$$

where q_t and q_e represent the amount of heavy metal ions adsorbed (mg g^{-1}) at time t (min) and the equilibrium time (min), respectively, and k_2 (g mg^{-1} min^{-1}) is the pseudo-second-order rate constant. The correlation coefficient (R^2) was relatively high (>0.996), and the calculated q_e values from the model fitting were very close to the experimental ones. These

Table 1. Kinetic Parameters for Metal Adsorption onto Fe_3O_4/MnO_2

metal	experimental q_e (mg g^{-1})	calculated q_e (mg g^{-1})	k_2 (g mg^{-1} min^{-1})	R^2
Pb(II)	9.81	9.85	0.367	0.999
Cu(II)	9.84	9.91	0.392	0.996
Zn(II)	8.01	8.15	0.160	0.997
Cd(II)	9.70	9.76	0.287	0.999

dx.doi.org/10.1021/am402615m | ACS Appl. Mater. Interfaces 2013, 5, 9628−9634

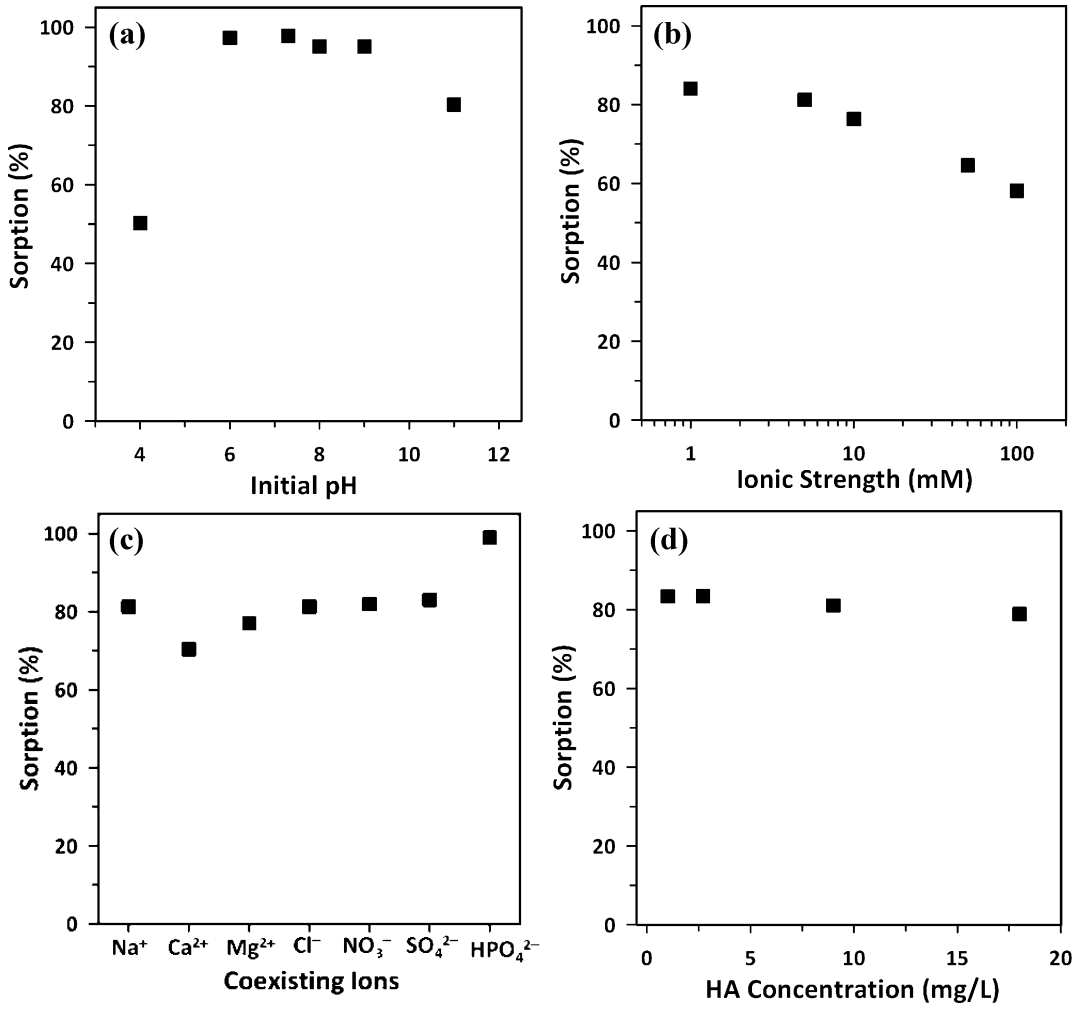

Figure 4. Sorption of Cd(II) on Fe_3O_4/MnO_2 under various solution conditions. Effects of (a) pH, (b) ionic strength, (c) coexisting ions (5 mM), and (d) HA concentration. ([Fe_3O_4/MnO_2], 1 g L^{-1}; [Cd(II)], 10 mg L^{-1}, pH 6.3 ± 0.1; contact time, 0.5 h).

results imply that the overall rate of the adsorption process is controlled by chemisorption rather than mass transport.[32] The adsorption rates of Fe_3O_4/MnO_2 for the four heavy metal ions were in the order of Cu(II) > Pb(II) > Cd(II) > Zn(II).

3.3. Effect of Solution Chemistry on the Adsorption of Cd(II). Cd(II) was chosen as a model adsorbate for further studies. Because of the complexity and variability of natural water and wastewater, it is highly necessary to investigate the adsorption capabilities of Fe_3O_4/MnO_2 under various solution chemistry conditions for the application in a practical treatment system. Therefore, we further examined the influences of pH, ionic strength, coexisting anion/cations, and the presence of HA on the removal of Cd(II) by the resulting composite.

The effect of the initial solution pH on Cd(II) adsorption by Fe_3O_4/MnO_2 is shown in Figure 4a, with the pH value ranging between 4.0 and 11.0 The sorption percentage of Cd(II) significantly increased upon increasing the pH from 4.0 to 6.0, and it then remained constant (~97%) in the pH range of 6.0–9.0. However, it reduced to 80% at pH 11.0. Fe_3O_4/MnO_2 exhibited a high adsorption capacity over a broad pH range. The dependence of Cd(II) uptake on pH can be interpreted by the relative distribution of Cd(II) species in solution and the surface chemistry of Fe_3O_4/MnO_2. Cd(II) in solution exists in several stable forms, such as Cd^{2+}, $Cd(OH)^+$, $Cd(OH)_2$, and $Cd(OH)_3^-$, and these forms are related to the solution pH and total Cd(II) concentration.[33] Cd^{2+} is predominantly present at pH ≤ 8.0, $Cd(OH)^+$ is the major form at pH > 8.0, and $Cd(OH)_2$ and $Cd(OH)_3^-$ are stable at pH > 10.0. Because Fe_3O_4/MnO_2 is negatively charged above pH 3.7 (cf. Figure 2b), the adsorption of the Cd(II) species is mainly governed by electrostatic attractions in the pH range of 4.0–11.0. Thus, $Cd(OH)_2$ and $Cd(OH)_3^-$ are difficult to be adsorbed on the Fe_3O_4/MnO_2 surface carrying negative charges, which explains the slight reduction of adsorption capacity at pH 11.

Figure 4b presents the removal of Cd(II) at various NaCl concentrations. It was observed that the sorption of Cd(II) gradually decreased as the ionic strength increased from 1 to 100 mM. The adverse effect of ionic strength is explained by two reasons: (i) the electrolyte ion (Na^+) competes with positively charged heavy metal ions for the same binding sites and (ii) the ionic strength influences the interfacial potential of heavy metals, which would in turn limit their transfer to the adsorbent surface.[34] The ionic strength dependence results provide molecular evidence for the formation of inner- vs. outer-sphere surface complexes. Outer-sphere complexation has proven to be more sensitive than inner-sphere complexes to the changes in ionic strength.[35] Our data suggest an outer-sphere adsorption mechanism for Cd(II).

The common ions present in natural water and wastewater may compete with the heavy metal ions for the available

dx.doi.org/10.1021/am402615m | ACS Appl. Mater. Interfaces 2013, 5, 9628–9634

Table 2. Equilibrium Parameters for Cd(II) Adsorption onto Fe_3O_4/MnO_2[a]

Langmuir model			Freundlich model			Temkin model		
$Q_e = \frac{Q_{max}K_LC_e}{1 + K_LC_e}$			$Q_e = K_FC_e^{1/n}$			$Q_e = \frac{RT}{b}\ln(A_TC_e)$		
Q_{max} (mg g^{-1})	K_L (L mg^{-1})	R^2	K_F (mg g^{-1})	n	R^2	A_T (L mg^{-1})	b	R^2
53.2	0.77	0.990	20.1	2.07	0.972	8.01	2.21×10^2	0.967

[a] C_e (mg L^{-1}) is the equilibrium concentration of metal, Q_e (mg g^{-1}) is the amount of metal adsorbed per weight unit of adsorbent at equilibrium, Q_{max} (mg g^{-1}) is the maximum adsorption capacity, K_L (L mg^{-1}) is the Langmuir adsorption equilibrium constant, K_F (mg g^{-1}) is the Freundlich constant representing the adsorption capacity, n (dimensionless) is the adsorption intensity, A_T (L mg^{-1}) is the Temkin equilibrium binding constant, and b (dimensionless) is the Temkin isotherm constant.

binding sites of adsorbents, affecting the adsorption process to some degree. On the basis of these reasons, we evaluated the influence of common electrolytes such as Ca^{2+}, Mg^{2+}, NO_3^-, SO_4^{2-}, and HPO_4^{2-} on Cd(II) removal by Fe_3O_4/MnO_2 (Figure 4c). Herein, the sample containing 5 mM NaCl was taken as a reference. The presence of coexisting cations resulted in a decrease in Cd(II) adsorption, and Ca^{2+} had a greater impact on this than did Na^+ and Mg^{2+}. Such a different competing capacity of the added cations may be due to their different electric charges and hydration energies. Generally, divelent cations are preferably adsorbed over monovalent ones, and divalent cations with a lower hydration energy are preferably adsorbed over those with a higher hydration energy.[36] For the coexisting anions, NO_3^- and SO_4^{2-} did not significantly impact the adsorption of Cd(II) to the composite compared with Cl^-. The surface of Fe_3O_4/MnO_2 at pH 6.3 ± 0.1 is negatively charged and is expected to repel the anions because of electrostatic repulsion. In contrast, it is interesting to note that the Cd(II) removal was greatly enhanced in the presence of HPO_4^{2-}. This can be related to the metal-like complexation reaction occurring at higher pH values. Above pH 6, the removal of Cd(II) from the aqueous solution in the presence of phosphate is dominated by precipitation of Cd-phosphate complexes ($CdHPO_4$), which in turn would result in nearly complete sorption of Cd(II).[37]

Humic substances that are primarily composed of humic and fulvic acids form most of the naturally occurring dissolved organic carbon in aquatic systems. Because humic substances are very active in binding metal ions in water, the interactions between the metal ions and adsorbent may vary depending on the presence or absence of humic substances.[38] Figure 4d shows the adsorption of Cd(II) as it is affected by different concentrations of HA. The addition of 1 mg L^{-1} HA reduced the Cd(II) adsorption, which was attributed to the competition between HA and Cd(II) for the available sorption sites of Fe_3O_4/MnO_2. In addition, the pH value in this study might also lead to a decrease in the Cd(II) sorption onto HA because HA tends to form weakly adsorbing complexes with Cd(II) at higher pH values. Further increases in the HA concentration, however, had a marginal influence on the removal of Cd(II). It was found that about 80% of the adsorption capacity of Fe_3O_4/MnO_2 was still retained even in the presence of 50 mg L^{-1} HA.

3.4. Sorption Isotherms of Cd(II). Different equilibrium models are often used to determine the adsorption behavior of an adsorbent. The equilibrium data for Cd(II) sorption were fitted by Langmuir, Freundlich, and Temkin models, respectively. The fitted results of all isotherm models are presented in Table 2. On the basis of the correlation coefficient values, it can be seen that the adsorption of Cd(II) was best described by the Langmuir model, suggesting that Cd(II) sorption was limited with monolayer coverage. In other words, the entire surface has identical sorption capacity and there is no significant interaction among adsorbed species. This may be attributed to the homogeneous distribution of surface hydroxyl groups on the composites and their mesopores. The maximum sorption capacity (Q_{max}) of Fe_3O_4/MnO_2 toward Cd(II) was 53.2 mg g^{-1}.

To evaluate the effectiveness of Fe_3O_4/MnO_2 as a potential sorbent for Cd(II), the Q_{max} value was compared with those of other sorbents reported in the previous literature (Table S1, Supporting Information).[24,39−46] The maximum adsorption capacity of Fe_3O_4/MnO_2 was higher or comparable than the values of alumina, carbon nanotube, and several surface-modified Fe_3O_4 nanoparticles with humic acid, cyclodextrin polymer, and mesoporous silica, but it was lower than that of pure graphene oxide and magnetic graphene oxide composite. Despite some great advantages of graphene oxide-based materials, the complicated synthetic procedure and high raw-material cost have obviously obstructed their wide applications. In contrast, Fe_3O_4/MnO_2 can be prepared by a simple and controllable method using cheap iron and manganese precursors. Moreover, the composite provides the separation convenience via external magnetic fields. It is worth noting that Fe_3O_4/MnO_2 is very stable under acidic conditions because the MnO_2 shell effectively protects the magnetic core from leaching out. For the above reasons, Fe_3O_4/MnO_2 can be considered as a promising sorbent for the efficient removal of heavy metals.

3.5. Regeneration of Saturated Fe_3O_4/MnO_2. From a practical/industrial point of view, the recycling and reuse of the adsorbent is an economic necessity. Taking into consideration that the composite exhibited a poor adsorption capacity at low pH, acid treatment is likely to be a suitable approach for the regeneration of Fe_3O_4/MnO_2. Herein, a 0.01 M HCl solution was used, and the desorption efficiency was found to be 90%.

The adsorption−desorption cycles were repeated five times using same batch of Fe_3O_4/MnO_2 (Figure 5a). As compared to the first adsorption, the removal efficiency at the fifth cycle decreased by about 12% to a value of 83%, indicating good regeneration and reusability. The slight decrease in the adsorption capacity was attributed to the incomplete desorption of Cd(II) from the surface of Fe_3O_4/MnO_2. For Cd(II) ions that go into the vacant site of MnO_2, desorption may be more difficult. After five cycles, the magnetic intensity of Fe_3O_4/MnO_2 did not decrease and the adsorbent could be separated from solution within 10 s. In addition, the leaching amount of Fe from the composite into the solution phase was nearly 0, indicating that the dissolution of the magnetic core under the stated experimental conditions was negligible. Figure 5b shows the representative SEM images of fresh and regenerated composites after the fifth cycle. Although the

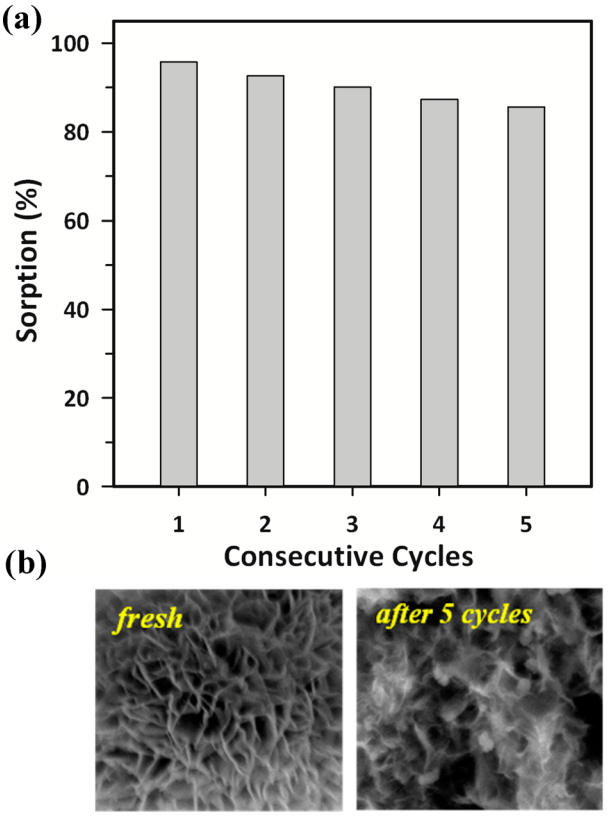

Figure 5. (a) Regeneration studies of Fe_3O_4/MnO_2 in the removal of Cd(II). ([Fe_3O_4/MnO_2], 1 g L^{-1}; [Cd(II)], 10 mg L^{-1}, pH 6.3 ± 0.1; contact time, 0.5 h). (b) SEM images of fresh and regenerated samples.

surface appeared rough and some broken spheres were observed, the regenerated composites still kept the flowerlike structure. Overall, our magnetic composite can be easily recycled and reused several times, which supports their long-term use in water purification.

4. CONCLUSIONS

An MnO_2-coated magnetic nanocomposite with a 3D flowerlike structure was successfully prepared by a facile hydrothermal method without using any template and organic surfactant. Fe_3O_4/MnO_2 was easily collected by an external magnetic field in a few seconds and could achieve a fast and efficient removal of different heavy metals (Cu(II), Pb(II), Zn(II), and Cd(II)) from water. The adsorption property was affected by certain hydrochemical conditions, especially low pH, high ionic strength, and the presence of calcium ions. Moreover, the composite could be recyclable up to five cycles without a significant decrease in its adsorption capacity. Considering the simple fabrication procedure, environmental friendliness, excellent removal capacity, and good regeneration performance of Fe_3O_4/MnO_2, it is expected that Fe_3O_4/MnO_2 has broad applications for the sorption and preconcentration of heavy metal ions from aqueous systems.

■ ASSOCIATED CONTENT

Supporting Information

Particle size distribution of Fe_3O_4/MnO_2 obtained from dynamic light scattering, energy-filtered TEM (EFTEM) images of Fe_3O_4/MnO_2, N_2 adsorption–desorption isotherm of Fe_3O_4/MnO_2, and comparison of the Cd(II) adsorption capacity of Fe_3O_4/MnO_2 with those of some other adsorbents reported in the literature. This material is available free of charge via the Internet at http://pubs.acs.org.

■ AUTHOR INFORMATION

Corresponding Author

*Phone: +82-54-279-2281; Fax: +82-54-279-8299; E-mail: yschang@postech.ac.kr.

Notes

The authors declare no competing financial interest.

■ ACKNOWLEDGMENTS

This work was supported by a National Research Foundation of Korea (NRF) grant funded by the Korea government (MEST) (no. 2012-0008787) and by The GAIA Project by the Korea Ministry of Environment.

■ REFERENCES

(1) Nriagu, J. O.; Pacyna, J. M. *Nature* **1988**, *333*, 134–139.
(2) Chen, Q.; Luo, Z.; Hills, C.; Xue, G.; Tyrer, M. *Water Res.* **2009**, *43*, 2605–2614.
(3) Gharabaghi, M.; Irannajad, M.; Azadmehr, A. R. *Ind. Eng. Chem. Res.* **2012**, *51*, 954–963.
(4) Vilensky, M. Y.; Berkowitz, B.; Warshawsky, A. *Environ. Sci. Technol.* **2002**, *36*, 1851–1855.
(5) Ritchie, S. M. C.; Kissick, K. E.; Bachas, L. G.; Sikdar, S. K.; Parikh, C.; Bhattacharyya, D. *Environ. Sci. Technol.* **2001**, *35*, 3252–3258.
(6) Celis, R.; HermosÍn, M. C.; Cornejo, J. *Environ. Sci. Technol.* **2000**, *34*, 4593–4599.
(7) Wingenfelder, U.; Hansen, C.; Furrer, G.; Schulin, R. *Environ. Sci. Technol.* **2005**, *39*, 4606–4613.
(8) Yuvaraja, G.; Subbaiah, M. V.; Krishnaiah, A. *Ind. Eng. Chem. Res.* **2012**, *51*, 11218–11225.
(9) Ali, I.; Gupta, V. K. *Nat. Protoc.* **2007**, *1*, 2661–2667.
(10) Ali, I. *Sep. Purif. Rev.* **2010**, *39*, 95–171.
(11) Ali, I.; Asim, M.; Khan, T. A. *J. Environ. Manage.* **2012**, *113*, 170–183.
(12) Ali, I. *Chem. Rev.* **2012**, *112*, 5073–5091.
(13) Ali, I. *Sep. Purif. Rev.* **2013**, *43*, 175–205.
(14) Peng, X.; Luan, Z.; Ding, J.; Di, Z.; Li, Y.; Tian, B. *Mater. Lett.* **2005**, *59*, 399–403.
(15) Gallego, M.; De Pena, Y. P.; Valcarcel, M. *Anal. Chem.* **1994**, *66*, 4074–4078.
(16) Rostamian, R.; Najafi, M.; Rafati, A. A. *Chem. Eng. J.* **2011**, *171*, 1004–1011.
(17) Mahdavi, S.; Jalali, M.; Afkhami, A. *Chem. Eng. Commun.* **2013**, *200*, 448–470.
(18) Liu, Y.; Su, G.; Zhang, B.; Jiang, G.; Yan, B. *Analyst* **2011**, *136*, 872–877.
(19) Mandel, K.; Hutter, F.; Gellermann, C.; Sextl, G. *ACS Appl. Mater. Interfaces* **2012**, *4*, 5633–5642.
(20) Farrukh, A.; Akram, A.; Ghaffar, A.; Hanif, S.; Hamid, A.; Duran, H.; Yameen, B. *ACS Appl. Mater. Interfaces* **2013**, *5*, 3784–3793.
(21) Shin, S.; Jang, J. *Chem. Commun.* **2007**, *0*, 4230–4232.
(22) Shi, S.; Fan, Y.; Huang, Y. *Ind. Eng. Chem. Res.* **2013**, *52*, 2604–2612.
(23) Zhu, J.; Wei, S.; Gu, H.; Rapole, S. B.; Wang, Q.; Luo, Z.; Haldolaarachchige, N.; Young, D. P.; Guo, Z. *Environ. Sci. Technol.* **2011**, *46*, 977–985.
(24) Liu, J.-F.; Zhao, Z.-S.; Jiang, G.-B. *Environ. Sci. Technol.* **2008**, *42*, 6949–6954.
(25) Liu, X.; Hu, Q.; Fang, Z.; Zhang, X.; Zhang, B. *Langmuir* **2008**, *25*, 3–8.
(26) Liu, R.; Liu, H.; Qiang, Z.; Qu, J.; Li, G.; Wang, D. *J. Colloid Interface Sci.* **2009**, *331*, 275–280.

(27) Zhu, M.; Farrow, C. L.; Post, J. E.; Livi, K. J. T.; Billinge, S. J. L.; Ginder-Vogel, M.; Sparks, D. L. *Geochim. Cosmochim. Acta* **2012**, *81*, 39−55.
(28) Post, J. E. *Proc. Natl. Acad. Sci. U.S.A.* **1999**, *96*, 3447−3454.
(29) Zhao, Z.; Liu, J.; Cui, F.; Feng, H.; Zhang, L. *J. Mater. Chem.* **2012**, *22*, 9052−9057.
(30) Xu, M.; Kong, L.; Zhou, W.; Li, H. *J. Phys. Chem. C* **2007**, *111*, 19141−19147.
(31) Caruntu, D.; Carnutu, G.; O'Connor, C. J. *J. Phys. D: Appl. Phys.* **2007**, *40*, 5801−5809.
(32) Sitko, R.; Turek, E.; Zawisza, B.; Malicka, E.; Talik, E.; Heimann, J.; Gagor, A.; Feist, B.; Wrzalik, B. *Dalton Trans.* **2013**, *42*, 5682−5689.
(33) Berber-Mendoza, M. S.; Leyva-Ramos, R.; Alonso-Davila, P.; Mendoza-Barron, J.; Diaz-Flores, P. E. *J. Chem. Technol. Biotechnol.* **2006**, *81*, 966−973.
(34) Reddad, Z.; Gerente, C.; Andres, Y.; Le Cloirec, P. *Environ. Sci. Technol.* **2002**, *36*, 2067−2073.
(35) Hayes, K. F.; Papelis, C.; Leckie, J. O. *J. Colloid Interface Sci.* **1988**, *125*, 717−726.
(36) Zaman, M. I.; Mustafa, S.; Khan, S.; Xing, B. *J. Colloid Interface Sci.* **2009**, *330*, 9−19.
(37) Lai, C.-H.; Chen, C.-Y.; Wei, B.-L.; Yeh, S.-H. *Water Res.* **2002**, *36*, 4943−4950.
(38) An, H. K.; Park, B. Y.; Kim, D. S. *Water Res.* **2001**, *35*, 3551−3556.
(39) Wang, Y.; Liang, S.; Chen, B.; Guo, F.; Yu, S.; Tang, Y. *PLoS One* **2013**, *8*, e65634-1−e65634-8.
(40) Badruddoza, A. Z. M.; Shawon, Z. B. Z.; Tay, W. J. D.; Hidajat, K.; Uddin, M. S. *Carbohydr. Polym.* **2013**, *91*, 322−332.
(41) Naiya, T. K.; Bhattacharya, A. K.; Das, S. K. *J. Colloid Interface Sci.* **2009**, *333*, 14−26.
(42) Li, Y.-H.; Ding, J.; Luan, Z.; Di, Z.; Zhu, Y.; Xu, C.; Wu, D.; Wei, B. *Carbon* **2003**, *41*, 2787−2792.
(43) Unob, F.; Wongsiri, B.; Phaeon, N.; Puanngam, M.; Shiowatana, J. *J. Hazard. Mater.* **2007**, *142*, 455−462.
(44) Zhao, G.; Li, J.; Ren, X.; Chen, C.; Wang, X. *Environ. Sci. Technol.* **2011**, *45*, 10454−10462.
(45) Tang, Y.; Liang, S.; Wang, J.; Yu, S.; Wang, Y. *J. Environ. Sci.* **2013**, *25*, 830−837.
(46) Wan, S.; Zhao, X.; Lv, L.; Su, Q.; Gu, H.; Pan, B.; Zhang, W.; Lin, Z.; Luan, J. *Ind. Eng. Chem. Res.* **2010**, *49*, 7574−7579.